Pergamon

Int. J. Heat Mass Transfer. Vol. 39, No. 3, pp. 491–501, 1996

0017-9310/96 $9.50+0.00

0017-9310(95)00147-6

Theory of thermal hydraulic quenchback

A. SHAJII and J. P. FREIDBERG†

Plasma Fusion Center, Massachusetts Institute of Technology, Cambridge, MA 02139, U.S.A.

(*Received* 12 *January* 1995 *and in final form* 5 *April* 1995)

Abstract—A theory is presented of a new heat propagation mechanism, thermal hydraulic quenchback (THQB), in large scale superconducting magnets. The underlying physics of THQB is discussed and an analytic solution for the quench propagation velocity is presented. This solution represents the first such result for THQB, and is shown to be in excellent agreement with the full numerical simulations of the governing mass, momentum, and energy conservation equations for the compressible flow of the coolant in the conduit. The THQB propagation velocity is observed to be as much as an order of magnitude greater than the helium coolant velocity. This is in direct contrast to a standard quench where the two velocities are always essentially equal.

1. INTRODUCTION

There are a number of large government and industrial projects that utilize superconducting magnets. Such projects include the magnetic fusion experiments, high energy particle accelerators, and magnetically levitated public transportation (MAGLEV). These magnets are particularly useful in situations where high magnetic fields are required but economic or technological considerations limit the total steady state electrical power available. Because of the high construction costs involved, magnet protection in the event of faults is a crucial design element. One of the most serious faults is that of quenching, a situation wherein a local section of the magnet, because of some local heat perturbation, returns to its normal state. If the perturbation is large enough, neighboring sections of the magnet are subsequently quenched. Late detection of quench invariably causes irreversible damage to the magnet. The purpose of this paper is to present a theory of a new quench (heat) propagation mechanism, thermal hydraulic quenchback (THQB), observed in recent superconducting magnet quench experiments [1]. The phenomenon occurs after the initiation of a 'standard' quench wherein the normal zone expands because of heat convection by the coolant. In certain circumstances a nearly explosive growth (by a factor on the order of 10) of the quench expansion velocity is suddenly observed at some point during the standard quench propagation. This highly enhanced propagation is known as thermal hydraulic quenchback.

The analysis presented here applies to the class of superconducting magnets constructed with Cable-in-Conduit Conductors (CICC), where THQB has been observed. A CICC consists of a superconducting cable surrounded by supercritical helium [2]. The helium is used to cool the superconductor during steady state operation. The system of helium and cable is surrounded by a conduit generally made of stainless steel. Figure 1 shows a schematic diagram of the cross-section of a CICC; typically the conduit has an overall diameter of the order of a few centimeters, while the conductor has a length of several hundred meters. The superconducting cable itself consists of a large number of strands (20–500) that enhance the heat transfer between the cable and the helium. These strands are made of a superconducting alloy embedded in a copper matrix. The alloy remains in its superconducting state when its temperature T lies below a critical value T_{cs}. Above T_{cs}, the alloy has a very high electrical resistivity. The copper matrix is used to carry the current in the event that the temperature in a section of the cable is accidentally raised above T_{cs}. In such a situation the current flows preferentially through the copper matrix which acts as a parallel resistor to the high resistivity, 'quenched' section of the superconducting alloy. This minimizes the Joule heating that would otherwise be present in the superconducting alloy alone. Even so, because of the high current density flowing in the cable, it often takes only a few seconds for the quenched section of the cable to rise from its cryogenic temperature $T \approx 5$ K and pressure $p \approx 5$ atm to values of $T \approx 250$ K and $p \approx 25$ atm. Past this point, irreversible damage to the magnet can occur. It is for this reason that understanding the process of quench propagation is of great importance in the construction of superconducting magnets.

The process of quench in CICC is discussed in [2–6], and in [3, 7] it has been shown that the helium in the conduit is the main component that governs the propagation. In a standard quench, the most common case, propagation is due to the convection of helium in the conduit. Reference [7] presents analytic results for this type of quench propagation, including an expression for the velocity of the quench front. In

† Author to whom correspondence should be addressed.

NOMENCLATURE

A	cross-sectional area
C_p	specific heat at constant pressure
C_t	specific heat of helium–conductor
C_v	specific heat at constant volume
C_α	$(1/T)\partial p(\rho, T)/\partial\rho$
C_β	$(1/\rho)\partial p(\rho, T)/\partial T$
c	specific heat ratio used in equation (46)
d_h	hydraulic diameter
F	function plotted in Fig. 6
f	friction factor
H	Heaviside step function
$\tilde{H}$	Heaviside-like function (Fig. 2)
J	current density in the copper
K	parameter given by equation (45)
K_1, K_2	parameters used in equation (43)
L	length of the channel
L_q	initial length of quench zone
$L_0 S_0^{2/3}$	parameter defined in equation (42)
l	scale length defined in equation (19)
p	helium pressure
R	ideal gas constant
S	Joule heating source
$\hat{S}$	entropy
T	temperature
T_{cr}	critical temperature
T_{cs}	current sharing temperature
T_m	maximum allowable temperature
ΔT	temperature margin defined in equation (26)
ΔT^*	$T_{cr} - T_{cs}$
t	time
t_{cr}	onset time of THQB
t_m	time scale to reach T_m
u	normalized velocity
v	helium velocity
v_s	sound speed in helium
V_q	velocity of the THQB front
V_{qs}	velocity of the standard quench front
w	re-normalized velocity used in equation (46)
x	distance along the channel
z	moving coordinate system.

Greek symbols

α	eigenvalue given by equation (23)
β	eigenvalue of equation (46)
ε	small expansion parameter, equation (10)
η	resistivity of copper
ρ	density
ξ	normalized moving coordinate system
ξ_0	parameter given by equation (30)
ξ_1	parameter given by equation (34)
ψ	normalized temperature used in equation (46).

Subscripts

c	denotes the conductor
cu	denotes the copper
h	denotes the helium
0	denotes a background (zeroth order) quantity
1	denotes a first order quantity.

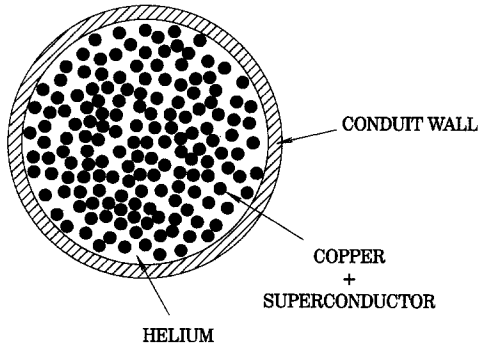

Fig. 1. Schematic of the cross-section of a CICC.

this paper, we discuss a different quench propagation mechanism due to the compression of helium in the conduit. This compression, which is driven by the standard quench, can cause the helium temperature to go above $T = T_{cs}$ in regions where the helium is nearly stagnant. As is shown, when this occurs the quench velocity is highly enhanced (i.e. the front velocity is much greater than the helium velocity) corresponding to THQB.

THQB has been observed in both numerical simulations [8, 9] and experiments [1]. Here, we present an explanation of the underlying physics of the process and derive an analytic expression for the velocity of the THQB normal front. The theory is shown to be in excellent agreement with new, more complete numerical simulations. It is in qualitative agreement with the experiments but there are insufficient data available as of now to make detailed comparisons.

2. THE GOVERNING MODEL

Consider the flow of supercritical helium in the conduit shown in Fig. 1. The radial length scale of the CICC has dimensions of ~ 0.1 m, while the length of the CICC is of the order of ~ 100 m. Therefore, use of one dimensional equations along the axial direction (x) of the CICC is well justified. For simplicity of presentation the conduit wall is assumed to be surrounded by a perfect insulator implying that

$\mathbf{n}\cdot\nabla T = 0$ on the conduit–insulator interface. Furthermore, the conduit wall is assumed to be negligibly thin (these assumptions have no essential bearing on any of the results presented in the paper).

Due to the small diameter of the strands, and the large heat transfer coefficient between the cable and the helium the temperatures of these components are nearly the same (this is particularly the case during quench time scales). Thus, it is possible to write a hybrid energy equation for the combined helium plus conductor system. In [6] the results of the hybrid equation are shown to compare very well with models that maintain separate temperatures for the cable and the helium. With this in mind, the governing equations for the flow consist of mass and momentum conservation equations for the helium coolant, and the hybrid energy conservation equation for the helium–conductor. These equations are given by [6]

$$\frac{\partial \rho}{\partial t} + \frac{\partial}{\partial x}(\rho v) = 0 \tag{1}$$

$$\frac{\partial p}{\partial x} = -\frac{f\rho v|v|}{2d_h} \tag{2}$$

$$\rho C_t \frac{\partial T}{\partial t} + \rho C_v v \frac{\partial T}{\partial x} + \rho C_\beta T \frac{\partial v}{\partial x} = S\tilde{H}(T - T_{cs}) + \frac{f\rho|v|v^2}{2d_h} \tag{3}$$

$$p = p(\rho, T) \tag{4}$$

where in equation (2) $f \approx 0.08$ is the friction factor, assumed to be a constant. The hydraulic diameter is defined as $d_h = 4A_h/P_w$, where A_h is the cross-sectional area of the helium and P_w is the total wetted perimeter. Also, helium inertia is neglected in this equation, since we are considering a low Mach number flow.

In equation (3) the second and third terms on the left-hand side represent convection and compressibility, respectively. The last term on the right-hand side represents the viscous heating. The specific heat of helium at constant volume is denoted by $C_v(\rho, T)$, and the compressibility coefficient $C_\beta(\rho, T) \equiv (1/\rho)\,\partial p(\rho, T)/\partial T$. Also observe that thermal conduction in the axial direction has been neglected in equation (3) since for the class of problems under consideration its effect is small compared to convection. The quantity C_t is the combined heat capacity of the helium and conductor, given by

$$C_t = C_v + \frac{A_c}{A_h}\frac{\rho_c}{\rho}C_c \tag{5}$$

where A_c and A_h denote the cross-sectional area of the conductor and the helium, respectively. Here, ρ_c is the conductor density, and $C_c(T)$ is the heat capacity of the conductor which is a strong function of temperature. Note that for $T \gtrsim 20$ K, the contribution of the specific heat of the solid components becomes substantial and dominates C_t, while for $T \lesssim 20$ K the helium contribution to C_t is the dominant term.

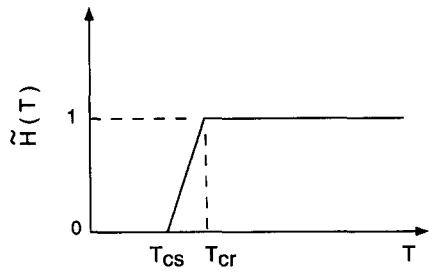

Fig. 2. Functional dependence of $\tilde{H}(T - T_{cs})$ appearing in equation (3).

The heat source appearing in the energy equation is due to the Joule heating in the copper. This heating takes place in regions where the superconductor is in the 'normal' (resistive) state, and is given by

$$S = \left(\frac{A_{cu}}{A_h}\right)\eta J^2 \tag{6}$$

where A_{cu} denotes the cross-sectional area of the copper. The quantity $\eta(T)$ is the resistivity of the copper, a strong function of the temperature in the range $T \gtrsim 20$ K. In the temperature range $T \lesssim 20$ K, however, η may be assumed to be a constant. Also, J is the current density in the copper, assumed to be constant. In equation (3), $\tilde{H}(T - T_{cs})$ is a Heaviside-like function such as used in [2], and T_{cs} is the so called 'current-sharing' temperature, above which the superconductor begins to share its current with the copper matrix. The functional dependence of $\tilde{H}$ is shown in Fig. 2. In the figure T_{cr} is the 'critical' temperature at which point all of the current is carried in the copper matrix. The current sharing and the critical temperatures are functions of the magnetic field B. In the paper we assume that B is uniform and constant.

In [6] it has been shown that equations (1)–(4) accurately describe quench propagation in CICC. In [7], several additional, well justified approximations are made, leading to a full analytic solution in the regime where the convection of helium is the dominant mechanism governing the propagation of heat (quench). In the next section we analyze a different quench propagation mechanism (THQB) which is due to the compression of the helium ahead of the initial quench zone. The propagation velocity in this case is shown to be greatly enhanced.

3. QUALITATIVE EXPLANATION OF THQB

During a standard quench, the front propagates away from the initial normal zone with a velocity $V_{qs} \sim 1$–10 m s^{-1}. Behind the front, the helium temperature rises quickly, well above the value T_{cr}, because of the Joule heating. Ahead of the front, there is no Joule heating and the helium remains essentially at its initial temperature $T_0 < T_{cs}$. Just ahead of the quench front, however, there is a slight increase in the temperature because of the compression of the helium

against the frictional drag force. A remarkable feature of the standard quench is that the temperature both behind and ahead of the front are independent of the values of T_{cs} and T_{cr}. In [7] it is shown that the temperature behind the standard quench front is mainly a function of the Joule heating S, while the temperature ahead of the front is a function of S as well as the friction f/d_h, the initial normal length L_q, and time. This situation persists until the temperature of the compressed helium just ahead of the front finally reaches the value T_{cs}. The Joule heating is then 'switched on' ahead, as well as behind the front and it is this sudden increase in heating power that causes the near explosive growth in the quench propagation velocity known as THQB.

The physical picture just described suggests the following analytic approach to understanding THQB. Consider a CICC undergoing a standard quench event and assume that the temperature just ahead of the quench has reached the value T_{cs}. This causes the initiation of a second quench front (i.e. the THQB front) because of the additional Joule heating. By fixing our position on the THQB front and analyzing the behavior of the helium ahead of this front it is possible to calculate the THQB propagation velocity. The calculation is made analytically tractable by utilizing two approximations. First, since THQB is fast compared to a standard quench, we can ignore the further evolution of the standard event. Second, since the current sharing and critical temperatures are often relatively close in value to the initial pre-quench temperature [i.e. $(T_{cs}-T_0)/T_0 < (T_{cr}-T_0)/T_0 \lesssim 1$], the behavior in the THQB region can be obtained by a perturbation analysis. The details of the analysis are described in Section 5.

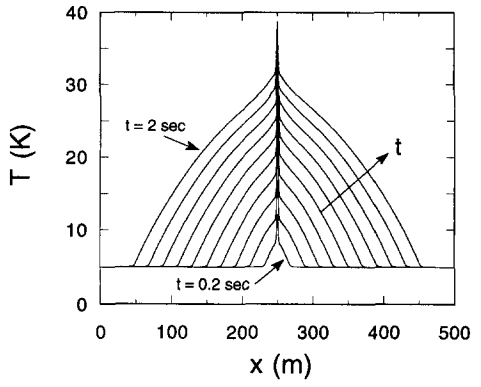

Fig. 3(a) Conductor–helium temperature profile at various times during THQB, obtained from the numerical solution of equations (1)–(4).

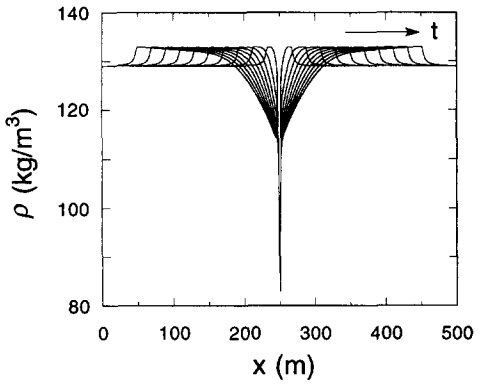

Fig. 3(b) Helium density profile at various times during THQB, obtained from the numerical solution of equations (1)–(4).

4. NUMERICAL RESULTS

Consider the helium coolant in a CICC of length L located between $0 \leqslant x \leqslant L$ to be initially ($t = 0$) stagnant, with a uniform temperature T_0 and density ρ_0. At $t = 0$ a localized external heat perturbation S_{ext} of sufficient magnitude is applied, causing the temperature at $x = L/2$ to rise above $T = T_{cs}$, thereby initiating Joule heating. For $t > 0$ the quench is at first propagated by convection of the helium. At a certain time t_{cr}, the compression of the helium just ahead of the front where $S = 0$, is sufficient to raise the temperature above $T = T_{cs}$. From this time forward the THQB propagation is governed by compression of helium ahead of the initial front.

The time t_{cr} has been derived in Ref. [8] and is given by

$$t_{cr} = 8.4\left(\frac{2d_h v_{s0}^8}{f}\right)\left[\frac{A_{cu}}{A_h}\frac{\rho_c C_c}{RL_q S}\right]^3\left(\frac{C_{v0}}{C_{\beta 0}}\frac{T_{cs}-T_0}{T_0}\right)^5$$

where v_{s0} is the speed of sound in helium, L_q is the initial normal length of the standard quench, R is the gas constant, and ρ_c, C_c are the density and specific heat of the conductor. Note that for a given quantity $Q(\rho, T)$, $Q_0 \equiv Q(\rho_0, T_0)$. Observe that t_{cr} is a strong function of $(T_{cs}-T_0)$. A related expression has been previously derived by Dresner [10]. His result applies to the regime where the heat capacity behind the front is dominated by the helium whereas in our case, the conductor dominates. This apparently simple difference leads to a significantly different scaling.

To motivate the analysis of Section 5 consider the nonlinear, time dependent numerical solution of a typical THQB event. In Figs. 3(a)–(d) we plot the helium temperature, density, velocity, and pressure profiles at various times during a 2 s THQB in a CICC similar to that used in the International Thermonuclear Experimental Reactor (ITER) [11] with $L = 500$ m. These figures represent the numerical solution of equations (1)–(4) obtained using the procedure described in [6]. The parameters of interest are $d_h = 5 \times 10^{-4}$ m and $f = 0.08$. The helium is initially stagnant ($v = 0$) with a temperature $T = T_0 = 5$ K and a density $\rho = \rho_0 = 129$ kg m^{-3}. At $t = 0$ an external heat source of a short duration (~ 0.1 s) is deposited over a 2 m length at $x = L/2$, in order to initiate the quench. The values of the transition temperatures are given by $T_{cs} = 5.1$ K, $T_{cr} = 5.5$ K, while

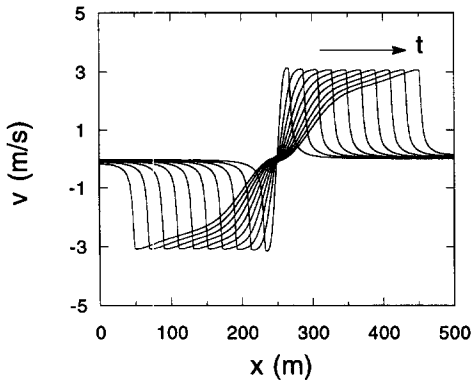

Fig. 3(c) Helium velocity profile at various times during THQB, obtained from the numerical solution of equations (1)–(4).

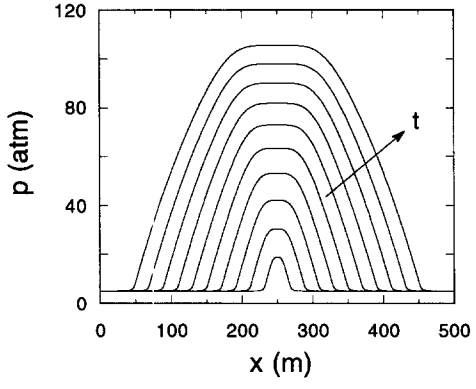

Fig. 3(d) Helium pressure profile at various times during THQB, obtained from the numerical solution of equations (1)–(4).

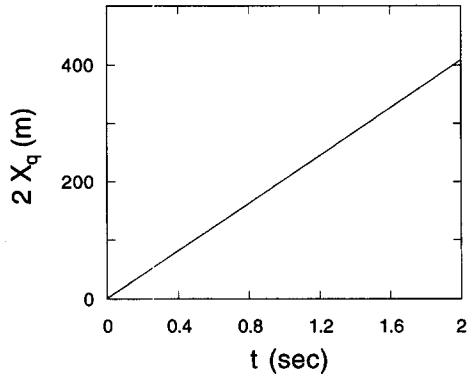

Fig. 4(a) Time evolution of normal length during a THQB with $\Delta T \equiv T_{cs} - T_0 = 0.1$ K, obtained from the numerical solution of equations (1)–(4).

the current density in the copper is $J = 10^8$ A m^{-2}. Also, $A_c = 6.1 \times 10^{-4}$ m^2, $A_{cu} = 3.9 \times 10^{-4}$ m^2, and $A_h = 4.5 \times 10^{-4}$ m^2. Observe how the THQB front rapidly separates from the initial standard quench front in the vicinity of $x = L/2$ as shown in Figs. 3(a) and (b). During THQB the boundary layer at the location of the standard front is nearly stagnant.

In Fig. 4(a) we present the time evolution of the

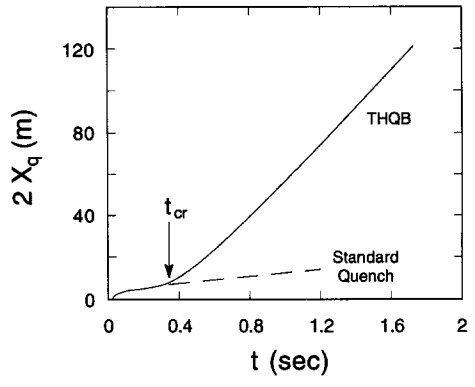

Fig. 4(b) Time evolution of normal length during a THQB with $\Delta T \equiv T_{cs} - T_0 = 1$ K, obtained from the numerical solution of equations (1)–(4).

length of the normal zone $2X_q$. After the onset of THQB, at $t = t_{cr}$, the normal front velocity quickly approaches a constant value given by $\dot{X}_q = V_q \approx 100$ m s^{-1}. This value of V_q is approximately an order of magnitude larger than the maximum helium velocity in the conduit [see Fig. 3(c)], while it is a factor of two smaller than the speed of sound in the helium. Also note that the value of t_{cr} in this case is very short (i.e. $t_{cr} \approx 0.01$ s) and consequently the sharp transition between the standard quench and THQB is barely visible in Fig. 4(a). In order to demonstrate this transition, we plot in Fig. 4(b) the time evolution of $2X_q$ for the case $T_{cs} = 6$ K and $T_{cr} = 6.4$ K. In this scenario $t_{cr} \approx 0.4$ s, $V_q \approx 45$ m s^{-1}, and $V_{qs} \approx 4$ m s^{-1}.

5. ANALYSIS

We now turn to the analysis. For simplicity of presentation the case $(T_{cs} - T_0)/T_0 \ll 1$ and $T_{cr} - T_{cs} \to 0$ is considered first in Section 5.1. In Section 5.2 the analysis is extended to cover all ranges of $(T_{cs} - T_0)/T_0$. The effect of finite $T_{cr} - T_{cs}$ on the quench propagation velocity is discussed in Section 5.3. Finally, modifications due to helium inertia are considered in Section 5.4.

5.1. *The case* $(T_{cs} - T_0)/T_0 \ll 1$

Due to the symmetry of the problem only the region $x \geqslant L/2$ needs to be treated. We define a new coordinate system moving with the THQB front: $z \equiv (x - L/2) - V_q t$, where $V_q = \text{const}$ is the velocity of the THQB normal front and is at this point unknown. Note that by construction, $z = 0$ is the location of the normal front. That is, $T(z = 0) \equiv T_{cs}$. In this coordinate system equations (1)–(4) can be written as

$$\frac{\partial \rho}{\partial t} + (v - V_q)\frac{\partial \rho}{\partial z} + \rho \frac{\partial v}{\partial z} = 0 \tag{7}$$

$$\frac{\partial p}{\partial z} = -\frac{f \rho v |v|}{2 d_h} \tag{8}$$

$$\rho C_t \frac{\partial T}{\partial t} + \rho(C_v v - C_t V_q)\frac{\partial T}{\partial z} + \rho C_\beta T \frac{\partial v}{\partial z} = S\tilde{H}(-z) + \frac{f\rho|v|v^2}{2d_h}. \quad (9)$$

For THQB, in general $V_q \gg v$, and the quench front is propagating into the region where the helium is nearly stagnant. Since $(T_{cs}-T_0)/T_0 \lesssim 1$, the helium temperature in this region is nearly the same as that of the background T_0. Similarly the density is approximately ρ_0. Therefore, for $z \gtrsim 0$ the following expansion is introduced to simplify equations (7)–(9)

$$T = T_0 + T_1(z,t) \quad (10a)$$

$$\rho = \rho_0 + \rho_1(z,t) \quad (10b)$$

$$v = v_1(z,t) \quad (10c)$$

where for a given quantity Q we have $Q_1/Q_0 \sim \varepsilon$. Here, $\varepsilon \equiv (T_{cs}-T_0)/T_0 < 1$. Also, we simplify the functional dependence of $\tilde{H}(T-T_{cs})$ by replacing it with an exact Heaviside function $H(T-T_{cs})$. In many practical cases $(T_{cr}-T_{cs})/(T_{cs}-T_0) < 1$, justifying the approximation. The effect of finite $(T_{cr}-T_{cs})/(T_{cs}-T_0)$ is discussed in Section 5.3.

Before proceeding, note that the zeroth order velocity component has been assumed to be zero. This is valid for sufficiently 'long coils' in which at the start of THQB the helium ahead of the front is unaffected by the ends and thus is nearly stagnant. The specific criterion for this to be valid is given by $L^2 > 24 d_h v_{s0}^2 t_{cr}/f V_{qs}(t_{cr})$, where V_{qs} is the standard quench propagation velocity for $t < t_{cr}$ given by the analytic results of [7]. Note that $V_{qs}(t_{cr})$ is generally much less than the value of V_q once THQB has been initiated [see Fig. 4(b)]. The leading order equations (7)–(9) can now be rewritten as

$$\frac{\partial \rho_1}{\partial t} - V_q \frac{\partial \rho_1}{\partial z} + \rho_0 \frac{\partial v_1}{\partial z} = 0 \quad (11)$$

$$\rho_0 C_{\beta 0}\frac{\partial T_1}{\partial z} + T_0 C_{\alpha 0}\frac{\partial \rho_1}{\partial z} = -\frac{f\rho_0}{2d_h}v_1^2 \quad (12)$$

$$\rho_0 C_{v0}\frac{\partial T_1}{\partial t} - \rho_0 C_{v0} V_q \frac{\partial T_1}{\partial z} + \rho_0 C_{\beta 0} T_0 \frac{\partial v_1}{\partial z} = SH(-z) \quad (13)$$

where $C_\alpha \equiv (1/T)\,\partial p(\rho,T)/\partial\rho$, and for a given quantity Q, $Q_0 \equiv Q(\rho_0, T_0)$. Observe that we have replaced C_t by the helium specific heat C_v in equation (13). In the region ahead of the front ($z \gtrsim 0$), $T \approx T_0$ and since typically $T_0 < 20$ K the helium contribution dominates C_t. Despite the expansion used, equations (11)–(13) are still non-linear because of the friction force; that is, the hydraulic diameter is sufficiently small so that friction dominates inertia. For mathematical consistency we thus assume $d_h S/f\rho_0 V_q^3 \sim \varepsilon^2$, and $(v_1/V_q) \sim \varepsilon$. Note that the frictional heating is a second order term and therefore does not appear in the energy equation.

To proceed we look for the steady state solution of equations (11)–(13) given by

$$-V_q \frac{d\rho_1}{dz} + \rho_0 \frac{dv_1}{dz} = 0 \quad (14)$$

$$\rho_0 C_{\beta 0}\frac{dT_1}{dz} + T_0 C_{\alpha 0}\frac{d\rho_1}{dz} = -\frac{f\rho_0}{2d_h}v_1^2 \quad (15)$$

$$-V_q \rho_0 C_{v0}\frac{dT_1}{dz} + \rho_0 C_{\beta 0} T_0 \frac{dv_1}{dz} = SH(-z). \quad (16)$$

These equations can be cast into a more useful form by introducing normalized variables as follows:

$$\xi \equiv z/l \quad (17)$$

$$u \equiv v_1/V_q \quad (18)$$

where the scale length l is defined as

$$l \equiv \frac{2d_h}{f}\frac{v_{s0}^2}{V_q^2} \quad (19)$$

and $v_{s0}^2 = T_0(C_{\alpha 0} + C_{\beta 0}^2/C_{v0})$ is the square of the sound speed. A simple calculation transforms equations (14)–(16) into a single equation for u and two subsidiary relations giving T_1 and ρ_1 in terms of u.

$$\frac{du}{d\xi} + u^2 = \alpha^2 H(-\xi) \quad (20)$$

$$\frac{d}{d\xi}\left(\frac{\rho_1}{\rho_0}\right) = \frac{du}{d\xi} \quad (21)$$

$$\frac{d}{d\xi}\left(\frac{T_1}{T_0}\right) = \frac{C_{\beta 0}}{C_{v0}}\left[\frac{du}{d\xi} - \alpha^2 \frac{C_{p0}}{C_{p0}-C_{v0}}H(-\xi)\right]. \quad (22)$$

Here, $C_{p0} = C_{v0} + C_{\beta 0}^2/C_{\alpha 0}$ is the specific heat at constant pressure and α^2 is defined as

$$\alpha^2 \equiv \frac{C_{\beta 0}}{C_{v0}}\frac{S}{(f/2d_h)\rho_0 V_q^3}. \quad (23)$$

The parameter $\alpha^2 = \alpha^2(V_q)$ is a nonlinear eigenvalue, which when evaluated determines the THQB propagation velocity V_q.

Equations (20)–(22) must be solved subject to the following boundary conditions

$$[v_1, \rho_1, T_1]_{z = L - V_q t \to \infty} \to 0 \quad (24)$$

$$[v_1, \rho_1, T_1]_{z = -V_q t \to -\infty} \to \textit{standard quench solution}. \quad (25)$$

The eigenvalue condition determining α^2 requires that

$$T_1|_{z=0} = T_{cs} - T_0 \equiv \Delta T. \quad (26)$$

Equation (24) implies that all perturbed quantities vanish far ahead of the THQB front. Equation (25) requires that the perturbed quantities match onto the standard quench solution far behind the THQB front. Equation (26) forces the temperature at the THQB front to equal the current sharing temperature, thereby defining the location of the THQB front.

The solution is obtained as follows. Ahead of the front (i.e. $\xi > 0$), $H(-\xi) = 0$. The resulting equations can easily be solved yielding

$$u = \frac{1}{\xi + \xi_0} \tag{27}$$

$$\frac{\rho_1}{\rho_0} = \frac{1}{\xi + \xi_0} \tag{28}$$

$$\frac{T_1}{T_0} = \frac{C_{\beta 0}}{C_{v0}} \frac{1}{\xi + \xi_0}. \tag{29}$$

Observe that the solutions satisfy the boundary conditions for $\xi \to \infty$. The parameter ξ_0 is an integration constant which is evaluated using the eigenvalue condition

$$\frac{1}{\xi_0} = \frac{C_{v0}}{C_{\beta 0}} \frac{\Delta T}{T_0}. \tag{30}$$

Behind the front (i.e. $\xi < 0$) $H(-\xi) = 1$. Here too the solution can be easily obtained

$$u = \alpha \tanh(\alpha\xi + \xi_1) \tag{31}$$

$$\frac{\rho_1}{\rho_0} = \alpha \tanh(\alpha\xi + \xi_1) \tag{32}$$

$$\frac{T_1}{T_0} = \frac{C_{\beta 0}}{C_{v0}} \left[\alpha \tanh(\alpha\xi + \xi_1) - \alpha^2 \frac{C_{p0}}{C_{p0} - C_{v0}} \xi \right] \tag{33}$$

where ξ_1 is an integration constant. In order for u, ρ_1 and T_1 to remain continuous across $\xi = 0$ we require

$$\alpha \tanh \xi_1 = \frac{1}{\xi_0}. \tag{34}$$

The parameter ξ_1 is in principle determined by matching equations (31)–(33) to the standard quench solution far behind the THQB front (i.e. at $z \approx -V_q t$). This is a difficult and subtle issue. The difficulties are two fold. First, at the standard quench front the temperature quickly rises well above the background value T_0 implying that the assumption $T_1 \ll T_0$ is no longer valid. Second, and more important, in the frame of the THQB front, the location of the standard quench front is rapidly receding away: z(standard front) $\approx -V_q t$. This moving boundary raises the question of whether or not it makes any sense to even consider a steady state solution.

The subtlety is that, while both of the above concerns are valid, they do not affect the determination of the THQB velocity. The reasoning is as follows: although we cannot explicitly determine ξ_1, the value required to match to the standard quench solution can be shown to satisfy $\xi_1 \gg 1$. This can be seen computationally in Fig. 5, obtained from a full nonlinear numerical solution of the THQB model. Illustrated here are profiles of v vs z in the THQB frame for different times. Observe that the solution ahead and slightly behind the THQB front are invariant (i.e. reach steady state), although they vary significantly near the standard quench front. To the extent that this assumption ($\xi_1 \gg 1$) is correct, then equation (34) reduces to

$$\alpha \approx \frac{1}{\xi_0} \tag{35}$$

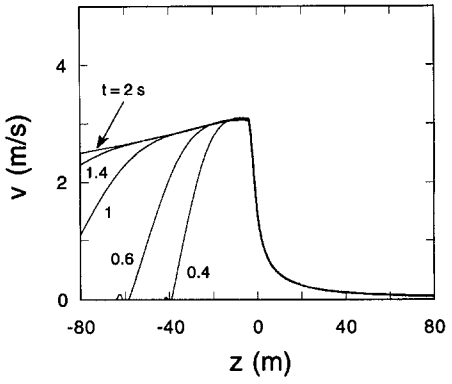

Fig. 5. Helium velocity profile in z-coordinates during THQB, obtained from the numerical solution of equations (1)–(4).

thereby determining the THQB propagation velocity. Note that under our assumption $\Delta T/T_0 \equiv \varepsilon \ll 1$, equation (30) implies that $\alpha \propto \Delta T/T_0 \ll 1$.

The condition $\xi_1 \gg 1$ can be analytically deduced from equation (33). We expect matching to occur when the hyperbolic tangent term in equation (33) exhibits a significant change in its value; that is, when $\xi_1 \sim \alpha|\xi_s|$ where ξ_s represents the characteristic distance to the standard quench front. As stated, the temperature at ξ_s rises significantly above T_0 once THQB is well established. A simple bound on ξ_s is thus obtained from equation (33) by balancing the second term on the right-hand side (the increasing term) with the left-hand side, setting $T_1 \sim T_0$. The result is

$$-\alpha^2 \xi_s \gtrsim 1 \tag{36}$$

which implies that $\xi_1 \sim 1/\alpha \gg 1$.

Under the condition $\xi_1 \gg 1$, the profiles just behind the THQB front ($\xi < 0$) simplify to

$$u \approx \alpha \tag{37}$$

$$\frac{\rho_1}{\rho_0} \approx \alpha \tag{38}$$

$$\frac{T_1}{T_0} \approx \frac{C_{\beta 0}}{C_{v0}} \left[\alpha - \alpha^2 \frac{C_{p0}}{C_{p0} - C_{v0}} \xi \right]. \tag{39}$$

The THQB propagation velocity follows from equations (35) and (30) and in un-normalized units is given by

$$V_q = \frac{C_{\beta 0}}{C_{v0}} \left(\frac{2 d_h S}{f \rho_0} \right)^{1/3} \left(\frac{T_0}{\Delta T} \right)^{2/3}. \tag{40}$$

This is the desired result. As expected, V_q increases with smaller temperature margin ΔT, or larger heating source $S = (A_{cu}/A_h)\eta_0 J^2$. Conversely, larger friction (f/d_h) results in smaller V_q since the compression term is proportional to v, and larger friction results in smaller helium velocities. Also note that V_q does not equal the speed of sound v_{s0}, nor is it bounded by v_{s0} as would be expected on physical grounds. Thus, infinite

front-velocities are allowed, for example, in the case where $\Delta T \to 0$. This breakdown of the model results from the neglect of the inertial term and is discussed in Section 5.4.

A final point of interest is to compare the THQB propagation velocity V_q to that of the standard quench velocity V_{qs}. A short calculation using the results of Ref. [7] yields

$$\frac{V_q}{V_{qs}} \approx \left(\frac{L_0 S_0^{2/3}}{L_q S^{2/3}}\right)^{2/5} \left(\frac{T_0}{\Delta T}\right)^{2/3} \tag{41}$$

where L_q is the length of the initial (standard) quench zone and $L_0 S_0^{2/3}$ is a parameter given by

$$L_0 S_0^{2/3} = 2.5\left(\frac{C_{\beta 0}}{C_{v0}}\right)^{5/2} \left(\frac{RT_m}{v_{s0}^2}\right)^{1/2} \times \left(\frac{A_{cu}}{A_h}\frac{\rho_c C_c}{\rho_0 R}\right)^{3/2} \left(\frac{d_h \rho_0^2 v_{s0}^6}{f}\right)^{1/3}. \tag{42}$$

Here, R is the gas constant, ρ_c and C_c are the density and specific heat of the conductor, and T_m is the maximum allowable temperature of the strongly heated zone behind the standard quench front. The quantity T_m appears because $V_{qs} \propto t^{-1/5}$, and t has been chosen as $t \approx t_m \approx (A_{cu}/A_h)\rho_c C_c T_m/S$, the time required for the hot zone to reach its maximum allowable temperature.

THQB is observed experimentally and computationally when the parameters are such that $V_q/V_{qs} \gg 1$. However, from equation (41) it is apparent that this inequality need not automatically be satisfied. In fact, for sufficiently large $L_q S^{2/3}$, $V_q/V_{qs} \lesssim 1$ implying that THQB cannot be initiated. The explanation is that as L_q and S increase, the propagation velocity of the standard quench increases faster than that of THQB. Eventually V_{qs} exceeds V_q and the THQB front cannot break away.

Interestingly, there is also a lower limit on $L_q S^{2/3}$ for the observance of THQB. For sufficiently small $L_q S^{2/3}$ the compressional heating is so small that the temperature behind the standard quench front reaches its maximum allowable value T_m before the onset of THQB. Consequently THQB can only be observed when $t_{cr} < t_m$. An alternate interpretation is that in a sufficiently long coil THQB will always be excited if one waits long enough for $T(z = 0^+)$ to compressionally heat to T_{cs}, provided that at this time T behind the front has not yet reached T_m; larger t_m makes it easier to observe THQB.

The two conditions just described define the approximate range of $L_q S^{2/3}$ for the appearance of THQB and can be expressed as

$$K_1\left(\frac{\Delta T}{T_0}\right)^{5/3} < L_q S^{2/3} < K_2\left(\frac{T_0}{\Delta T}\right)^{2/3}$$

$$K_1 = 2.6\left(\frac{C_{v0}}{C_{\beta 0}}\right)^{5/3} \left(\frac{v_{s0}^2}{RT_m}\right)^{1/3} \left(\frac{A_{cu}}{A_h}\frac{\rho_c C_c}{\rho_0 R}\right)^{2/3} \left(\frac{d_h \rho_0^2 v_{s0}^6}{f}\right)^{1/3}$$

$$K_2 = 2.5\left(\frac{C_{\beta 0}}{C_{v0}}\right)^{5/2} \left(\frac{RT_m}{v_{s0}^2}\right)^{1/2} \left(\frac{A_{cu}}{A_h}\frac{\rho_c C_c}{\rho_0 R}\right)^{3/2} \left(\frac{d_h \rho_0^2 v_{s0}^6}{f}\right)^{1/3}. \tag{43}$$

To summarize, we have calculated the velocity of propagation of THQB [equation (40)] and the conditions under which it occurs [equation (43)]. In addition two approximations have been used which define the region of validity of the analysis. First, we have assumed $\Delta T/T_0 \ll 1$ in order to carry out the perturbation analysis. Second, we have assumed that $L \gg V_q t_m$ to insure that the coil is sufficiently long so as to be unaffected by end effects. Next, we consider the modification to equation (40) when $\Delta T/T_0 \sim 1$.

5.2. *The case* $(T_{cs} - T_0)/T_0 \sim 1$

Equation (40) is valid in the limit $\Delta T/T_0 \ll 1$. In practice, this parameter can sometimes be as large as 0.5. Thus, while (40) remains qualitatively correct for larger $\Delta T/T_0$, its quantitative value becomes progressively less accurate. It would be clearly useful to have a more accurate value for comparison with experiments and numerical simulations. In this regard the previous analysis can be re-derived for the full nonlinear equations including convection and frictional heating. The analysis is slightly tedious, but if one assumes that $\Delta T/T_0$ is small, the first-order correction to equation (40) can be calculated analytically. The result is

$$V_q = \frac{C_{\beta 0}}{C_{v0}}\left(\frac{2d_h S}{f\rho_0}\right)^{1/3} \left(\frac{T_0}{\Delta T}\right)^{2/3} \left(1 + K\frac{\Delta T}{T_0}\right) \tag{44}$$

where

$$K = 2 + \frac{C_{v0}}{C_{\beta 0}} + \frac{C_{p0}}{C_{p0} - C_{v0}} - 2\left[\frac{\partial \ln (C_{v0}/C_{\beta 0})}{\partial \ln T_0}\right]_{\hat{S}}. \tag{45}$$

Note that the derivative in equation (45) is carried out at fixed entropy $\hat{S}$.

5.3. *Effect of finite* $T_{cr} - T_{cs}$

The derivation of the THQB propagation velocity assumes that $(T_{cs} - T_0)/T_0 < 1$ and $(T_{cr} - T_0)/(T_{cs} - T_0) \to 0$. The first condition is often well satisfied experimentally. The second condition is more problematic, but has been used anyway for mathematical simplicity. In this section we extend the previous analysis to include finite $(T_{cr} - T_0)/(T_{cs} - T_0)$.

The analysis ahead of the surface $T = T_{cs}$ and behind the surface $T = T_{cr}$ are the same as in Section 5.2 since the equations remain unchanged in these regimes. What we require now is a solution in the intermediate region $T_{cs} < T < T_{cr}$. By properly matching at both ends we obtain a more general expression for V_q.

In the intermediate region one can easily derive, from equations (20) and (22), a differential equation relating v to T assuming the transition source function

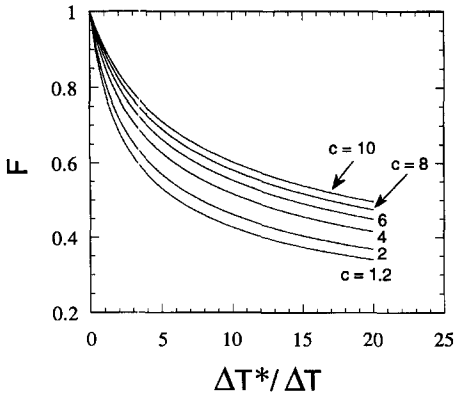

Fig. 6. Functional dependence of F appearing in equation (47).

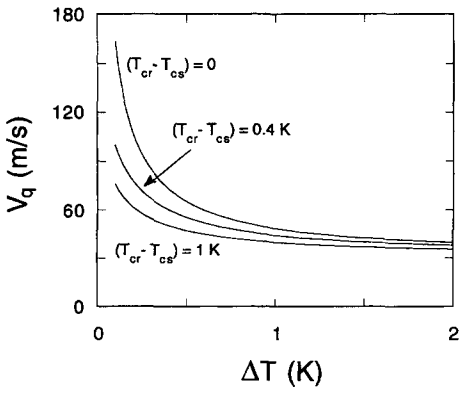

Fig. 7. Propagation velocity V_q vs $\Delta T \equiv T_{cs}-T_0$ for different values of $\Delta T^* \equiv T_{cr}-T_{cs}$.

$\tilde{H}(T-T_{cs})$ is linear in T, as shown in Fig. 2. This equation is given by

$$\frac{dw}{d\psi}=\frac{\Delta T^*}{\Delta T}\left[\frac{w^2-\beta^2\psi}{w^2+(c-1)\beta^2\psi}\right] \tag{46}$$

where the new normalized quantities are defined as $w=\xi_0 u$, $\psi=(T_1-\Delta T)/\Delta T^*$, $\beta=\alpha\xi_0$, $\Delta T^*=T_{cr}-T_{cs}$ and $c=C_{p0}/(C_{p0}-C_{v0})$. The normalizations have been chosen so that $0\leqslant\psi\leqslant 1$ and at $\psi=0$, $w(0)=1$. The eigenvalue condition determining β requires that at $\psi=1$, $w(1)=\beta$.

Equation (46) has been solved numerically for given values of $\Delta T^*/\Delta T$ and c to obtain β. The result, in unnormalized units is an expression for V_q of the form

$$V_q=\frac{C_{\beta 0}}{C_{v0}}\left(\frac{2d_h S}{f\rho_0}\right)^{1/3}\left(\frac{T_0}{\Delta T}\right)^{2/3}F\left(\frac{\Delta T^*}{\Delta T},c\right). \tag{47}$$

The function F is plotted in Fig. 6 as a set of universal curves. Observe that the basic scaling dependences of V_q remain unchanged, but that there are important quantitative changes in its magnitude as $\Delta T^*/\Delta T$ varies. These corrections are necessary when comparing with either experimental or numerical simulations in which $\Delta T^*/\Delta T$ is often finite.

Equation (47) can be easily modified to approximately include the additional finite $\Delta T/T_0$ corrections as follows:

$$V_q=\frac{C_{\beta 0}}{C_{v0}}\left(\frac{2d_h S}{f\rho_0}\right)^{1/3}\left(\frac{T_0}{\Delta T}\right)^{2/3}\left(1+K\frac{\Delta T}{T_0}\right)F\left(\frac{\Delta T^*}{\Delta T},c\right). \tag{48}$$

Equation (48) is used later to compare with the numerical results.

The combined effects of the finite ΔT and ΔT^* corrections are illustrated in Fig. 7 where we have plotted V_q vs ΔT for various ΔT^* corresponding to the ITER-like coil. Observe that for small ΔT the $\Delta T^*/\Delta T$ corrections are important, but the $K\Delta T/T_0$ corrections are by definition negligible. Conversely, for larger ΔT, the $K\Delta T/T_0$ corrections become important, but as seen by the convergence of the curves, the $\Delta T^*/\Delta T$ corrections become unimportant. Consequently, for any given set of parameters, one or the other correction may be dominant, but not both simultaneously.

5.4. *Inertial effects*

As has been previously noted, the value of $V_q\to\infty$ as $S\to\infty$ or $\Delta T\to 0$. Realistically, we expect some change in the physics to occur when $V_q\approx v_{s0}$, preventing V_q from increasing without bound. In this section we include inertial effects and show that for physical solutions to exist $V_q<v_{s0}$.

Within the context of the perturbation analysis, the effect of inertia modifies the steady state momentum equation [equation (15)] as follows:

$$\rho_0 V_q\frac{dv_1}{dz}+\rho_0 C_{\beta 0}\frac{dT_1}{dz}+T_0 C_{\alpha 0}\frac{d\rho_1}{dz}=-\frac{f\rho_0}{2d_h}v_1^2. \tag{49}$$

The first term is the inertial correction. The equivalent normalized equations [equations (20)–(22)] now have the form

$$\left(1-\frac{V_q^2}{v_{s0}^2}\right)\frac{du}{d\xi}+u^2=\alpha^2 H(-\xi) \tag{50}$$

$$\frac{d}{d\xi}\left(\frac{\rho_1}{\rho_0}\right)=\frac{du}{d\xi} \tag{51}$$

$$\frac{d}{d\xi}\left(\frac{T_1}{T_0}\right)=\frac{C_{\beta 0}}{C_{v0}}\left[\frac{du}{d\xi}-\alpha^2\frac{C_{p0}}{C_{p0}-C_{v0}}H(-\xi)\right]. \tag{52}$$

The only modification from the original equations is the $(1-V_q^2/v_{s0}^2)$ coefficient in equation (50).

Following the analysis in Section 5.1 we again calculate the eigenvalue α^2. Remarkably, in the simple limit $\Delta T^*\to 0$, the value of α^2 is unchanged from the case where inertia is neglected: $\alpha=(C_{v0}/C_{\beta 0})(\Delta T/T_0)$. However, the functional dependence of u ahead of the THQB front is modified as follows

$$u=\frac{1-V_q^2/v_{s0}^2}{\xi+(1-V_q^2/v_{s0}^2)\xi_0}. \tag{53}$$

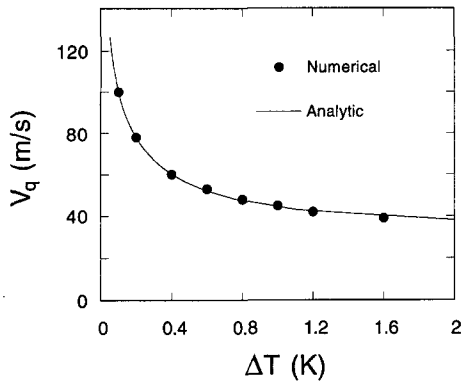

Fig. 8. Comparison of analytic and numerical results for V_q vs $\Delta T \equiv T_{cs} - T_0$. Here, $\Delta T^* \equiv T_{cr} - T_{cs} = 0.4$ K.

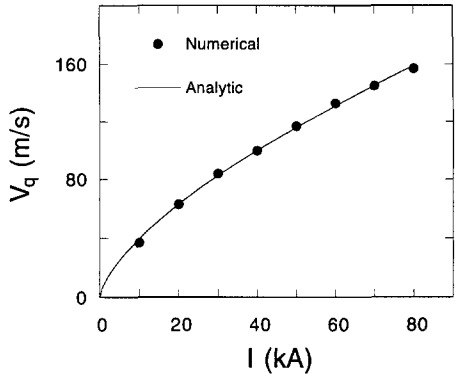

Fig. 9. Comparison of analytic and numerical results for V_q vs $I = A_{cu}J$. Here, $\Delta T \equiv T_{cs} - T_0 = 0.1$ K and $\Delta T^* \equiv T_{cr} - T_{cs} = 0.4$ K.

Observe that when $V_q^2 < v_{s0}^2$ the solutions are well behaved. For $V_q^2 > v_{s0}^2$, the denominator vanishes for $\xi = (V_q^2/v_{s0}^2 - 1)\xi_0 > 0$ indicating non-physical behavior.

The conclusion is that the value of V_q given by equation (40) is correct and independent of inertia as long as $V_q^2 < v_{s0}^2$ (i.e. when $S/\Delta T^2$ is sufficiently small). If $S/\Delta T^2$ is increased above the value that gives $V_q = v_{s0}$, a shock-like solution develops. The velocity, temperature and density develop jumps across the THQB front which is thereafter constrained to move at v_{s0}. This regime is generally not the normal operating regime of most CICC magnets.

6. DISCUSSION

Consider the conductor discussed in relation to Figs. 3 and 4. For this conductor we compare the analytic results with the numerical solution of equations (1)–(4). Recall that for this case $\Delta T^* = 0.4$ K, $T_0 = 5$ K, $\rho_0 = 129$ kg m^{-3}, $C_{v0} = 2522$ J kg^{-1} K^{-1}, $C_{\beta 0} = 3344$ J kg^{-1} K^{-1}, $d_h = 5 \times 10^{-4}$ m, $f = 0.08$, $S = 6.8 \times 10^6$ W m^{-3}, $c = 2.1$ and $K = 2.18$. In Fig. 8 we plot V_q as a function of ΔT. The analytic solution, given by equation (48), is in good agreement with the numerical results. Note that approximately 10 h of CPU time was required on an Alpha station (DEC 3000/600) to obtain the computational data presented in Fig. 8. This relatively large computational cost is a result of needing to resolve two moving boundary layers at the location of the THQB and standard quench fronts (see Fig. 3). Relative to the length of the channel, the layer-width at the THQB front is $\sim 1\%$ (see Fig. 5).

In Fig. 9 we plot V_q vs I for the case $\Delta T = 0.1$ K and $\Delta T^* = 0.4$ K. Here, I is the conductor current given by $I = A_{cu}J$. Again, we observe good agreement between the numerical and analytic results.

Due to preliminary nature of experiments, we cannot compare the THQB theory developed here with any detailed experimental data. A challenging future step to further investigate THQB is to perform careful experiments where V_q is measured and compared to the results of the paper. An important factor in performing such a task is to keep in mind that the results obtained here apply to 'long coils' where compressional heating is the dominant factor governing THQB (this is the main case of interest corresponding to large scale superconducting magnets with $L^2 > 24 d_h v_{s0}^2 t_{cr}/f V_{qs}$). In short coils ($L^2 < 24 d_h v_{s0}^2 t_{cr}/f V_{qs}$), the frictional heating governs both the initiation and the propagation of THQB [8], and the propagation velocity is equal to the sound speed in helium. To estimate the transition value of L^2/d_h from a short to a long coil, consider typical values of $v_{s0} \approx 200$ m s^{-1}, $V_{qs} \approx 1$ m s^{-1}, $f \approx 0.08$ and $t_{cr} \approx 1$ s, which results in $L^2/d_h \approx 10^7$ m. In a long coil experiment, L^2/d_h must be greater than this transition value.

In conclusion, we have presented an analytic theory for the process of THQB in large scale superconducting magnets made of CICC. The analytic solution for the quench propagation velocity is in good agreement with numerical results, where various scaling relations have been compared. Also, V_q is shown to be governed by the temperature margin ΔT, Joule heating $\eta_0 J^2$, and friction d_h/f. In general, V_q is observed to be much greater than the helium velocity, while its value is substantially below the sound speed. Future experiments are required to further verify the results presented in the paper.

Acknowledgements—The authors would like to thank the members of the Engineering Division at MIT's Plasma Fusion Center, particularly Dr E. A. Chaniotakis, for many useful discussions during the course of the work.

REFERENCES

1. J. W. Lue, L. Dresner, S. W. Schwenterly, C. T. Wilson and M. S. Lubell, Investigating thermal hydraulic quenchback in a cable-in-conduit superconductor, *IEEE Trans. Appl. Superconductivity* **3**, 338–341 (1993).
2. M. N. Wilson, *Superconducting Magnets*. Oxford University Press, New York (1983).
3. L. Dresner, Protection considerations for forced-cooled superconductors, *11th Symposium on Fusion Engineering, IEEE Proceedings*, Vol. 2, pp. 1218–1222 (1986).
4. L. Bottura and O. C. Zienkiewicz, Quench analysis of

large superconducting magnets, Parts I and II, *Cryogenics* **32,** 659 (1992).
5. T. Ando, M. Nishi, T. Kato, J. Yoshida, N. Itoh and S. Shimamoto, Propagation velocity of the normal zone in a cable-in-conduit conductor, *Advances in Cryogenic Engineering*, Vol. 35, pp. 701–708. Plenum Press, New York (1990).
6. A. Shajii and J. P. Freidberg, Quench in superconducting magnets—I. Model and numerical implementation, *J. Appl. Phys.* **76,** 3149–3158 (1994).
7. A. Shajii and J. P. Freidberg, Quench in superconducting magnets—II. Analytic solution, *J. Appl. Phys.* **76,** 3159–3171 (1994).
8. A. Shajii, Theory and modelling of quench in cable-in-conduit superconducting magnets, Ph.D. Thesis, Massachusetts Institute of Technology (1994).
9. C. A. Luongo, R. J. Loyd, F. X. Chen and S. D. Peck, Thermal hydraulic simulation of helium expulsion from a cable-in-conduit conductor, *IEEE Trans. Magn.* **MAG-25,** 1589–1595 (1989).
10. L. Dresner, Theory of thermal hydraulic quenchback in cable-in-conduit superconductors, *Cryogenics* **31,** 557–561 (1991).
11. R. J. Thome, Magnet program overview for the international experimental test reactor, *IEEE Trans. Mag.* **MAG-30,** 1595–1601 (1994).